

Large electromechanical response in ferroelectrics: Beyond the morphotropic phase boundary paradigm

Uma Shankar,¹ Naveen Kumar,¹ Bastola Narayan,¹ Diptikanta Swain,² Anatoliy Senyshyn,³ and Rajeev Ranjan^{1,*}

¹*Department of Materials Engineering, Indian Institute of Science, Bangalore-560012, India*

²*Solid State Structural Chemistry Unit, Indian Institute of Science, Bangalore-560012, India*

³*Forschungsneutronenquelle Heinz Maier-Leibnitz (FRM II), Technische Universität München, Lichtenbergstrasse 1, D-85747 Garching bei München, Germany*



(Received 3 May 2019; revised manuscript received 10 August 2019; published 3 September 2019)

Ferroelectric based piezoceramics exhibiting large electromechanical response are used as sensors, actuators, and transducers in wide-ranging applications spanning sectors like space, defense, medical diagnostics, etc. In general, the large piezoelectric response in ferroelectric solid solutions is associated with a composition driven interferroelectric instability, commonly known as a morphotropic phase boundary (MPB). Here, we show that MPB is not necessarily required to achieve electromechanical response equivalent to, or even more than what can be achieved in MPB based ferroelectric solid solutions. We show this on two ferroelectric solid solution systems, namely, $(1-x)\text{PbTiO}_3\text{-}(x)\text{Bi}(\text{Ni}_{1/2}\text{Hf}_{1/2})\text{O}_3$ (PT-BNH) and $(\text{Bi}, \text{La})\text{FeO}_3\text{-PbTiO}_3$ (BF-PT:La) which show large piezoelectric response ($d_{33} \sim 450$ pC/N) and extraordinarily high electrostrain of $\sim 1.3\%$, respectively. Although analogous to the conventional MPB systems, the critical compositions of these two alloys mimic a two-phase structural state (cubic + tetragonal), detailed analysis that suggests that it is not so. The cubic phase is rather a manifestation of short correlation length of the tetragonal regions and appears when the system is compositionally driven from a normal ferroelectric state to a relaxor ferroelectric state. This proves that, in contrast to conventional MPB systems, the large electromechanical response of the critical compositions of PT-BNH and BF-PT:La is not due to interferroelectric instability enabled polarization rotation. In the absence of the MPB, the sole contributor to large electromechanical response is a process associated with domain wall motion, large local polarization, and (non-MPB) lattice softening. The generalized ideas derived from our investigation offer scope for expanding the basket of high-performance piezoelectric materials by exploring solid solutions outside of the MPB framework.

DOI: [10.1103/PhysRevB.100.094101](https://doi.org/10.1103/PhysRevB.100.094101)

I. INTRODUCTION

Ever since the discovery that electromechanical response is enhanced at the morphotropic phase boundary (MPB) of the pseudobinary ferroelectric alloy system $\text{PbTiO}_3\text{-PbZrO}_3$ (PZT) [1], MPB has been the guiding principle in search of materials with large electromechanical response [2–6]. In the composition-temperature phase diagram of a pseudobinary ferroelectric system, MPB separates two different ferroelectric phase regions (say rhombohedral and tetragonal), and represents a composition driven interferroelectric instability. The anisotropic flattening of the free energy profile at the MPB leads to enhanced propensity for polarization rotation on application of external electric field/stress [7,8]. In the framework of the polarization rotation model [7] the large electromechanical response at the MPB is considered as an intrinsic lattice response. The nearly flattened free energy profile at the MPB also reduces the energy of the domain walls and favors domain miniaturization [9]. The enhanced mobility of the domain walls also contributes significantly to the enhancement of the electromechanical response at the MPB [10,11]. This aspect is more important in polycrystalline ceramics

which are necessarily in the multidomain state to minimize the stress within the grains due to the clamping effect [10].

While the concept of polarization rotation is central to MPB, domain miniaturization is a more general phenomenon. For example, irrespective of whether MPB exists or not, all relaxor ferroelectrics show polar-nano-regions, (PNRs) [12] which impart special properties to the system. Some of the MPB systems such $\text{Pb}(\text{Zn}_{1/3}\text{Nb}_{2/3})\text{O}_3\text{-PbTiO}_3$ (PZN-PT) and $\text{Pb}(\text{Mg}_{1/3}\text{Nb}_{2/3})\text{O}_3\text{-PbTiO}_3$ (PMN-PT) show features of relaxor ferroelectricity and are well known for their ultrahigh electromechanical response [2]. In the scenario when MPB is not formed within the solid solution regime during alloying of a ferroelectric compound, it is most likely to degenerate into a relaxor state with miniaturized domains. While a fully developed relaxor state shows electrostrictive behavior with a low value of saturation polarization, the crossover regime, wherein the system exhibit mixed tendencies, can be of special interest regarding piezoelectric properties, and deserves systematic exploration. A pertinent question is whether MPB is mandatory for large electromechanical response, or even whether non-MPB ferroelectric systems can also show large electromechanical response as the conventional MPB systems. Here we have taken two ferroelectric solid solutions, namely, $(1-x)\text{PbTiO}_3\text{-}(x)\text{Bi}(\text{Ni}_{1/2}\text{Hf}_{1/2})\text{O}_3$, (PT-BNH) [13] which is analogous to $(1-x)\text{PbTiO}_3\text{-}(x)\text{Bi}(\text{Ni}_{1/2}\text{Zr}_{1/2})\text{O}_3$

*rajeev@iisc.ac.in

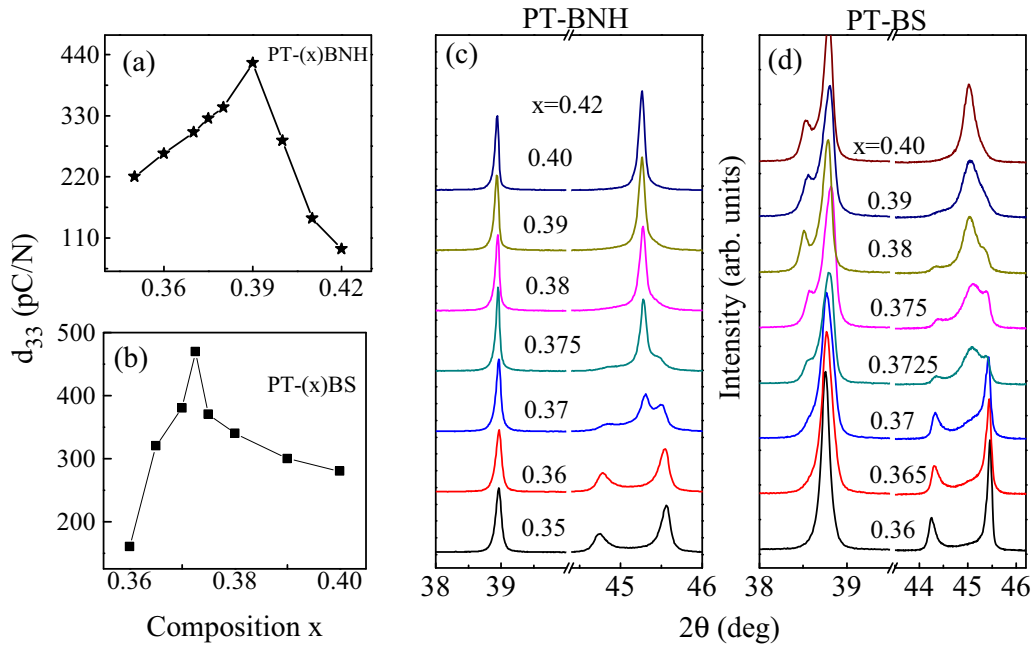


FIG. 1. Composition dependence of the piezoelectric coefficient (d_{33}) of (a) $(1-x)$ PT- (x) BNH, and (b) $(1-x)$ PT- (x) BS. (c,d) show the composition evolution of the pseudocubic $\{111\}_{pc}$ and $\{200\}_{pc}$ XRD Bragg profiles of unpoled powder specimens of $(1-x)$ PT- (x) BNH and $(1-x)$ PT- (x) BS.

(PT-BNZ) [14], and $(\text{Bi, La})\text{FeO}_3\text{-PbTiO}_3$ (BF-PT:La) [15] as model examples, and demonstrate that they do not show MPB. Yet they exhibit large electromechanical response, like that of the conventional MPB piezoelectrics, in the normal-relaxor crossover regime. One of these non-MPB systems, BF-PT:La, shows an extraordinarily large electrostrain, 1.3%, which is much higher than that shown by any MPB based piezoelectric.

II. EXPERIMENTAL SECTION

The specimens of $(1-x)\text{PbTiO}_3\text{-}(x)\text{Bi}(\text{Ni}_{1/2}\text{Hf}_{1/2})\text{O}_3$ [PT-BNH], $(1-x)\text{PbTiO}_3\text{-}(x)\text{BiScO}_3$ [PT-BS], and $(1-x)\text{Bi}_{1-y}\text{La}_y\text{FeO}_3\text{-}(x)\text{PbTiO}_3$ [BF-PT:La] were prepared by the conventional solid-state sintering method. High-purity analytical grade Bi_2O_3 , PbO , NiO , HfO_2 , La_2O_3 , Sc_2O_3 , and TiO_2 (99.8%, Alfa Aesar) raw materials (purity >99.5%) chemicals were wet milled according to stoichiometric proportions in a zirconia jar with zirconia balls and acetone as the wetting agent for 6 h using a planetary ball mill (Fritsch P5). The thoroughly mixed powder was calcined at 900°C for 6 h and then milled again by the same process in order to make the powder finer and more uniform. The calcined powder was mixed with a 2 wt% polyvinyl alcohol-water solution and pressed into the form of disks of 15 mm diameter by using a uniaxial die at 100 MPa, followed by sintering at $\sim 1200^\circ\text{C}$ 2 h under ambient conditions in a closed alumina crucible with precalcined spare powder. Density measurements on the sintered specimens were carried out using the Archimedes principle. All pellets showed a density of $\sim 95\%$ of the theoretical density. The powder x-ray ($\text{Cu } K\alpha_1$ radiation; $\lambda = 1.5406 \text{ \AA}$) diffraction pattern of the sintered pellets was crushed into fine powder and annealed at 500°C for 6 h to remove the strains introduced during crushing. X-ray powder diffraction (XRD) was

performed using a Rigaku (SMART LAB) diffractometer with a Johansson monochromator in the incident beam to remove the $\text{Cu } K\alpha_2$ radiation contribution. The sintered specimen revealed peaks corresponding to the perovskite phases only confirming the complete solid solubility of these compositions. The longitudinal piezoelectric coefficient (d_{33}) was measured by poling the pellets at room temperature for 1 h at a dc electric field of $\sim 40.0 \text{ kV/cm}$ using a Piezotest PM-300. Dielectric measurement was carried out using the Novocontrol (Alpha-A) impedance analyzer. Total x-ray scattering data were collected at the powder diffraction synchrotron beamline P02.1 at PETRA III at DESY with incident beam energy of 60 keV and the pair distribution functions were obtained through Fourier transformation using the PDFGETX3 package [16].

III. RESULTS AND DISCUSSION

A. Unpoled $\text{PbTiO}_3\text{Bi}(\text{Ni}_{1/2}\text{Hf}_{1/2})\text{O}_3$ and $\text{PbTiO}_3\text{-BiScO}_3$

Figure 1(a) shows the composition dependence of the weak-field piezoelectric coefficient (d_{33}) of PT-BNH. It is important to note that the large $d_{33} \sim 450 \text{ pC/N}$ of the critical PT-BNH composition ($x = 0.39$) is comparable [Fig. 1(b)] to that of the MPB composition of the pseudobinary solid solution $(1-x)\text{PbTiO}_3\text{-}(x)\text{BiScO}_3$ (PT-BS) [17,18]. This provided a good opportunity for a comparative structural study of critical compositions of PT-BNH and PT-BS. The x-ray powder diffraction study was carried out by grinding the sintered pellets ($\sim 95\%$ density) to powder and subsequently annealing to remove the effect of residual stress incurred during the grinding process. Such specimens are called here “unpoled specimens.” XRD measurements were also done on powder obtained from poled pellets (poled specimens). Figures 1(c) and 1(d) show the composition evolution of

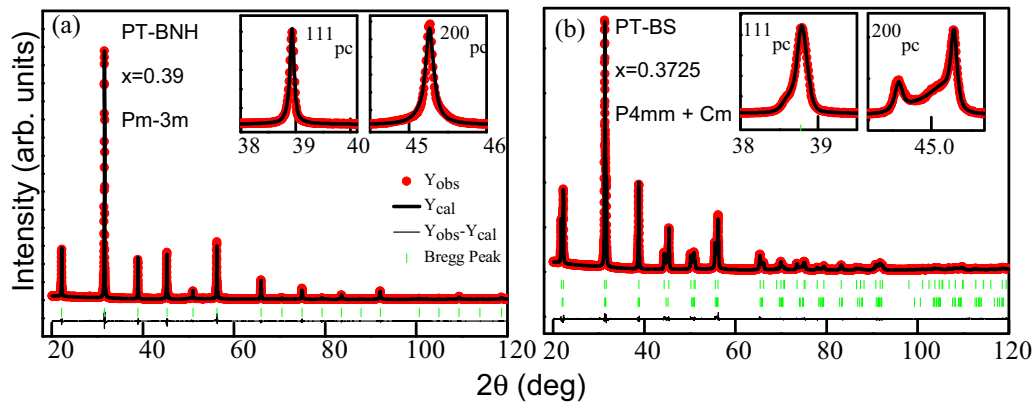


FIG. 2. Rietveld fitted XRD pattern of the critical compositions of (a) PT-BNH ($x = 0.39$) and (b) PT-BS ($x = 0.3725$). The PT-BNH pattern is fitted with the cubic ($Pm\bar{3}m$) structural model. The PT-BS pattern is fitted with the $P4mm + Cm$ phase coexistence model. The $P4mm$ and the Cm Bragg positions are shown by the upper and lower vertical bars, respectively.

the pseudocubic $\{111\}_{pc}$ and $\{200\}_{pc}$ XRD Bragg profiles of unpoled PT-BNH and PT-BS. The $PbTiO_3$ -rich compositions (say $x = 0.36$ of both PT-BS and PT-BNH) exhibit tetragonal, $P4mm$ structure as evident from the doublet nature of the $\{200\}_{pc}$ and the singlet nature of the $\{111\}_{pc}$. With increasing x , the $\{200\}_{pc}$ becomes triplet in both cases (e.g., $x = 0.375$ of both systems). The $\{111\}_{pc}$ profile, however, remains singlet for all compositions of PT-BNH (the XRD pattern suggests a cubiclike phase for higher BNH compositions; $x = 0.40$). In contrast, the BS-rich composition of PT-BS ($x = 0.40$) exhibit a rhombohedral/monoclinic structure as evident from the splitting of the $\{111\}_{pc}$. It is interesting to note that the XRD pattern of the critical composition ($x = 0.39$) of PT-BNH exhibiting maximum piezoelectric response ($d_{33} \sim 450$ pC/N) exhibits a cubic phase. The pattern could be nicely fit with the cubic ($Pm\bar{3}m$) structural model as shown in Fig. 2(a). In contrast, the XRD pattern of the critical composition of PT-BS ($x = 0.3725$) could be fitted only by considering the coexistence of tetragonal ($P4mm$) and monoclinic (Cm) structures, Fig. 2(b) [17].

B. Poled $PbTiO_3$ - $Bi(Ni_{1/2}Hf_{1/2})O_3$ and $PbTiO_3$ - $BiScO_3$

Given the similarity of d_{33} (~ 450 pC/N) of PT-BNH and PT-BS, the question is the following: Is the cubiclike phase in PT-BNH equivalent to the rhombohedral phase of PT-BS? If this is so, the structural scenario of the critical composition of PT-BNH can be reconciled within the the MPB framework. Now, if the ground-state structure of the composition exhibiting the cubic phase is rhombohedral, we anticipate a strong electric field to reveal this phase on the global scale by increasing the correlation length of the rhombohedral ferroelectric regions. Dielectric measurements confirmed that they are all in their nonergodic state at room temperature, Fig. 3. The field-stabilized long-range ferroelectric order is therefore expected to be irreversible to a large extent when poled at room temperature. This precludes the necessity for *in situ* XRD measurements with an electric field for determining the ground-state structure (revealed on the global scale assisted by the electric field). The *ex situ* field XRD measurements of (poled) specimens can equally ascertain the symmetry of the ferroelectric phase in the nonergodic state. For the sake

of better appreciation of the usefulness of this strategy, we performed the same exercise on the MPB ($x = 0.3725$) and the rhombohedral composition ($x = 0.40$) of PT-BS.

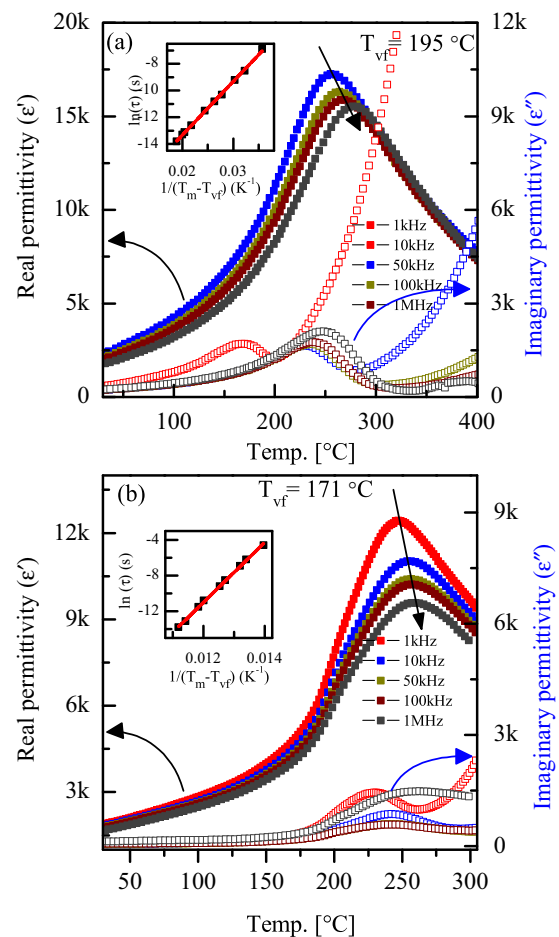


FIG. 3. Temperature dependence of the real and imaginary permittivity of the critical composition of (a) PT-BNH ($x = 0.39$), and (b) BF-PT: La ($y = 0.30$). The Vogel Fulcher fits are shown in the respective inset. The freezing temperatures (T_{vf}) in all cases are above room temperature confirming the room temperature state to be nonergodic.

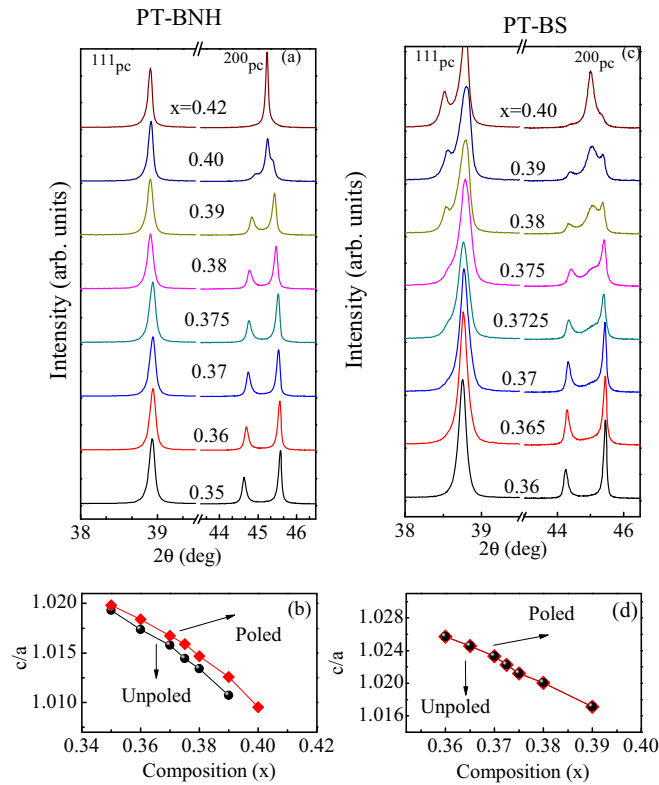


FIG. 4. (a) Pseudocubic $\{111\}_{pc}$ and $\{200\}_{pc}$ Bragg profiles of XRPD patterns of poled PT-BNH. (b) Composition dependence of the tetragonality of poled and unpoled PT-BNH. (c) Pseudocubic $\{111\}_{pc}$ and $\{200\}_{pc}$ Bragg profiles of XRPD patterns of poled PT-BS. (d) Composition dependence of the tetragonality of poled and unpoled PT-BS.

In our approach, the poled pellets were ground to powder to get rid of preferred orientation induced by domain switching. This helps in unambiguous interpretation of the structural changes via the changes observed in the shape of the Bragg profiles [19]. Subsequent diffraction measurements on poled pellets concurred with these conclusions. Figure 4 shows the composition evolution of the two characteristic pseudocubic profiles $\{111\}_{pc}$ and $\{200\}_{pc}$ of poled PT-BNH and PT-BS. The two-phase ($T + R$) state of the composition exhibiting maximum piezoelectric response of PT-BS ($x = 0.3725$) is retained after poling, the only difference being that poling decreases the fraction of the rhombohedral/monoclinic phase by $\sim 15\%$. There is no noticeable change in the XRD pattern of the rhombohedral PT-BS composition $x = 0.40$ after poling. In contrast, the cubic phase of the critical composition ($x = 0.39$) of PT-BNH transforms to tetragonal after poling. The next higher composition ($x = 0.40$) also show cubic to tetragonal transformation after poling, though the extent of transformation is far less than that in $x = 0.39$, Fig. 4(a). Assuming that composition driven structural evolutions in PT-BS and PT-BNH are similar, and that the cubic phase of PT-BNH is representative of short-range rhombohedral correlations, then poling should make the rhombohedral phase manifest on the global scale by increasing its correlation length. That is, the $\{111\}_{pc}$ Bragg profile of PT-BNH should have split into two for $x = 0.39$ and $x = 0.40$. This contrasts with our

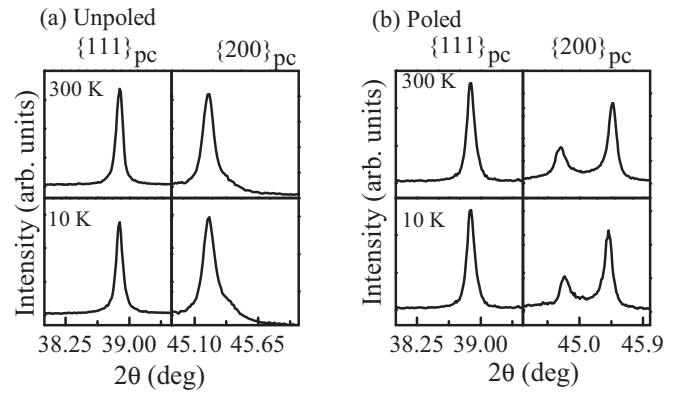


FIG. 5. Pseudocubic $\{111\}_{pc}$ and $\{200\}_{pc}$ XRD Bragg profiles of critical composition ($x = 0.39$) of (PT-BNH) (a) unpoled and (b) poled at 300 and 10 K. The singlet nature of the $\{111\}_{pc}$ both in the unpoled and poled specimens confirms the tetragonal ground state of the critical composition of PT-BNH.

observations which show $\{111\}_{pc}$ as a singlet. Figures 4(b) and 4(d) show the compositional dependence of tetragonality (c/a) of poled and unpoled samples of PT-BNH and PT-BS, respectively. The tetragonality of poled samples is higher than that of annealed samples of PT-BNH. In contrast, there is no noticeable change in the tetragonality after poling the MPB system PT-BS (MPB).

Diffraction patterns of PT-BNH collected at 10 K also did not reveal any symptom of rhombohedral distortion both in the unpoled and poled specimens (Fig. 5), thereby confirming that the tetragonal phase observed at room temperature is also the ground-state structure. The next higher composition, $x = 0.42$, remains cubic even after poling. In view of the remarkable drop in d_{33} (~ 100 pC/N) for this composition, it implies that the overall ferroelectric character of this composition is considerably weakened, presumably due to the dominating influence of the random fields. The same behavior was observed for the analogous system PT-BNZ [14]. Our results suggest that unlike PT-BS, PT-BNH has no tendency to stabilize the rhombohedral phase. The critical compositions exhibiting maximum piezoelectric response are therefore not associated with MPB in PT-BNH. We performed local structure analysis to understand the changes on the local scale, if any, associated with the poling induced cubic to tetragonal transformation in PT-BNH. A distinct change in the relative PDF intensity of distances corresponding to the average A-O and A-B bonds before and after poling of PT-BNH suggests a poling induced rearrangement in bonds on the local scale, Fig. 6. In contrast, the MPB composition of PT-BS does not show a noticeable change in the local structure.

C. $\text{BiFeO}_3\text{-PbTiO}_3\text{:La}$

Next, we present the results of the pseudoternary system $\text{BiFeO}_3\text{-PbTiO}_3\text{-LaFeO}_3$. This system was reported recently [15]. However, we deem it fit to discuss the extraordinary electromechanical response of this ferroelectric solid solution for the sake of highlighting large electromechanical response in non-MPB ferroelectric systems. The specimens were prepared

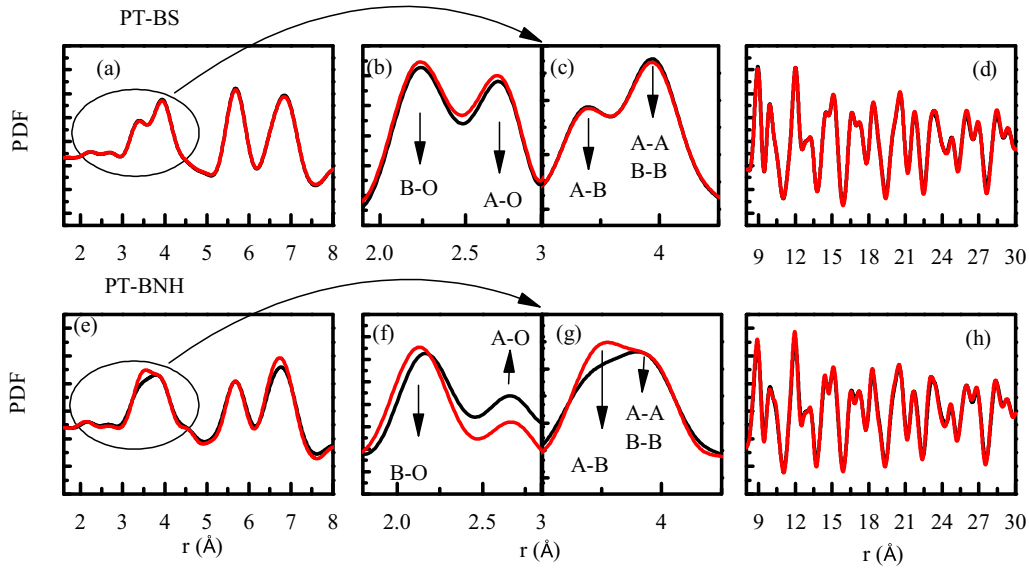


FIG. 6. (a–d) Synchrotron x-ray pair distribution function (PDF) pattern of unpoled (black) and poled (red) PT-BS ceramic ($x = 0.3725$) for two different ranges of r (Å). (b) Magnified view of the part of the PDF pattern highlighting B - O and A - O correlations for unpoled and poled specimens. (c) Magnified view of the part of the PDF pattern highlighting A - B and A - A or B - B correlations for unpoled and poled specimens. (e–h) PDF pattern of unpoled and poled PT-BNH ($x = 0.39$) for two different ranges of r (Å). (f) Magnified view of the part of the PDF pattern highlighting B - O and A - O correlations for unpoled and poled specimens. (g) Magnified view of the part of the PDF pattern highlighting A - B and A - A or B - B correlations for unpoled and poled specimens.

as per the nominal formula $(1-x)\text{Bi}_{1-y}\text{La}_y\text{FeO}_3-(x)\text{PbTiO}_3$ in a wide composition space (x, y). The La-free series, namely, $(1-x)\text{BiFeO}_3-(x)\text{PbTiO}_3$, is well known for its very large tetragonality ($c/a \sim 1.19$) for $x \sim 0.30$ [20], negative/nearly zero thermal expansion coefficient [21], isostructural transformation [22,23], and size driven interferroelectric transformation on a very large length scale [24]. We have focused on the composition $x = 0.45$ which, like the two cases discussed above (PT-BNH and PT-BNZ), exhibit a tetragonal to cubic transformation with increasing La concentration. The evolution of the XRD pattern of $0.55\text{Bi}_{1-y}\text{La}_y\text{FeO}_3-0.45\text{PbTiO}_3$ with La concentration (y) shown in Fig. 7(a) confirms this transformation for $y > 0.25$ in unpoled specimens. The cubic and the tetragonal phases coexist in the composition range $0.27 \leq y \leq 0.32$. The maximum d_{33} (~ 350 pC/N) was obtained for $y = 0.30$ [Fig. 7(b)]. The most remarkable property, however, is the ultrahigh unipolar electrostrain of $\sim 1.3\%$ for the same composition [Fig. 7(c)]. This value is comparable to what has so far been achieved only in single crystals [2]. The unpoled critical composition shows a cubiclike phase, Fig. 7(a). After poling the cubiclike peaks almost disappear, exactly mimicking the scenario as that in critical composition of PT-BNH [Fig. 7(d)] and PT-BNZ [14]. The ultrahigh electrostrain is therefore associated with this field-stabilized tetragonal phase. The monotonic decrease of the tetragonal cell volume with La concentration shown in Fig. 7(e) is consistent with the smaller radius of La^{+3} (1.16 Å) with respect to that of Bi^{+3} (1.17 Å) [25]. The tetragonality decreases systematically with increasing La concentration, Fig. 7(f). For the critical concentration the tetragonality is $\sim 2.5\%$. This value is more than double the tetragonality of pure BaTiO_3 (1.1%). As discussed below, the large tetragonality of the critical composition of BF-PT:La is of great significance in ensuring the large electrostrain.

We ascertained the mechanism associated with the ultrahigh electrostrain by carrying out structural investigation *in situ* with an electric field using XRD. In Bragg-Brentano diffraction geometry the Bragg peaks are contributed by surface grains whose (hkl) planes are nearly parallel to the flat sample surface exposed to the x-ray beam. The electric field was applied across the thickness of a Au sputter-coated disk. The planes contributing to the Bragg peaks are those which experience an electric field normal to them. To be consistent with the unipolar electrostrain measurements the XRD measurements *in situ* with an electric field was carried out on a poled pellet of BF-PT:La ($y = 0.30$). Since the poled specimens are tetragonal with a very small fraction of the residual cubic phase, the domain switching and lattice strain (and not the field dependent interferroelectric transformation [26]) are expected to be the sole factors contributing to the ultrahigh electrostrain of $y = 0.30$. For the tetragonal ferroelectric phase, field driven switching of the ferroelectric-ferroelastic switching of domains can be ascertained by monitoring the relative intensity of the $(002)_T$ and $(200)_T$ tetragonal peaks as shown in Fig. 8(a). It is interesting to note that the relative intensity of the two peaks obtained from the poled pellet is nearly the same as for a preferred orientation free powder pattern of the tetragonal specimen. This implies that poling has not induced significant preferred orientation in this specimen. The domain reorientation fraction (η) by the poling field was estimated using the expression [11]

$$\eta_{002} = \frac{\frac{I_{002}}{I'_{002}}}{\frac{I_{002}}{I'_{002}} + 2\frac{I_{200}}{I'_{200}}} - \frac{1}{3}, \quad (1)$$

where I_{002} and I_{200} are the integrated intensities in the presence of an electric field and I'_{002} and I'_{200} are the integrated

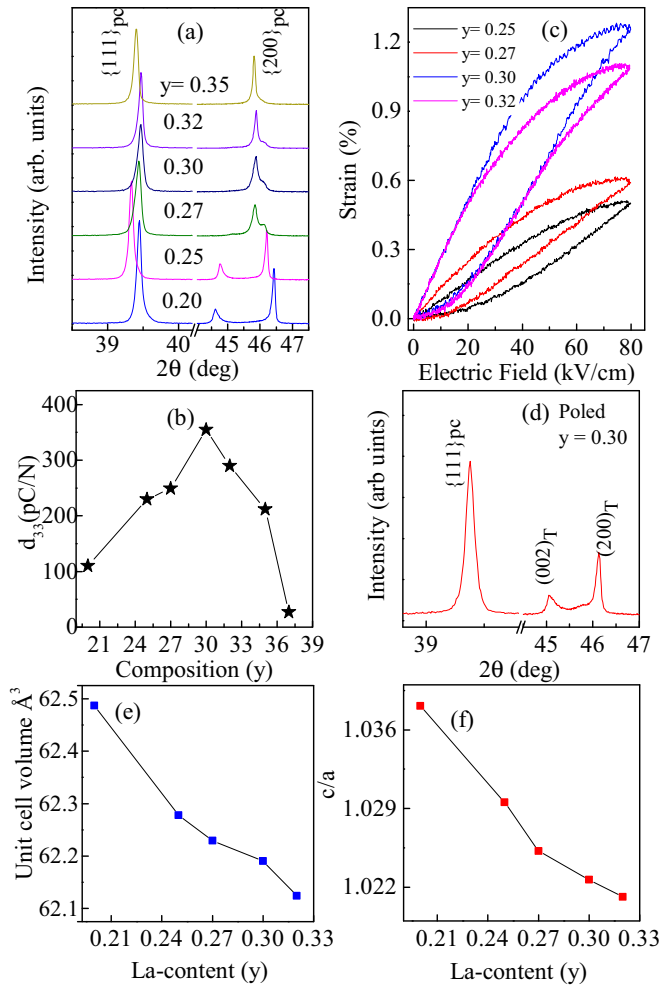


FIG. 7. (a) Composition evolution of the pseudocubic $\{111\}_{pc}$ and $\{200\}_{pc}$ XRD Bragg profiles of unpoled $0.55\text{Bi}_{1-y}\text{La}_y\text{FeO}_3\text{-}0.45\text{PbTiO}_3$ (BF-PT:La). (b,c) show the composition dependence of piezoelectric coefficient (d_{33}) and unipolar electrostrain, respectively. (d) $\{111\}_{pc}$ and $\{200\}_{pc}$ XRD Bragg profiles of critical composition of poled and ground BF-PT:La ($y = 0.30$). (e,f) show the composition dependence of the tetragonal unit cell volume and tetragonality, respectively.

intensities before application of an electric field for the $\{002\}_T$ and $\{200\}_T$ Bragg peaks, respectively.

After poling the domain switching fraction (with respect to the random orientation) is merely 0.10. This is an abnormally small value not generally observed in normal ferroelectric systems. While moving under the influence of a strong electric field, the domain walls generally get pinned by randomly distributed defects and do not acquire the random configuration after switching off the field, leading to preferred orientation. The small value of η in our poled specimen suggests the existence of a strong depinning force comparable to the attractive force between the defects and the domain walls. On application of the field, the intensity of $\{002\}_T$ gradually increases with respect to that of $\{200\}_T$. At a field of 60 kV/cm, η reaches ~ 0.4 . It decreases back to 0.10 after the field is switched off. The total switching fraction obtained at 60 kV/cm in the poled specimen is therefore 0.3%. Interest-

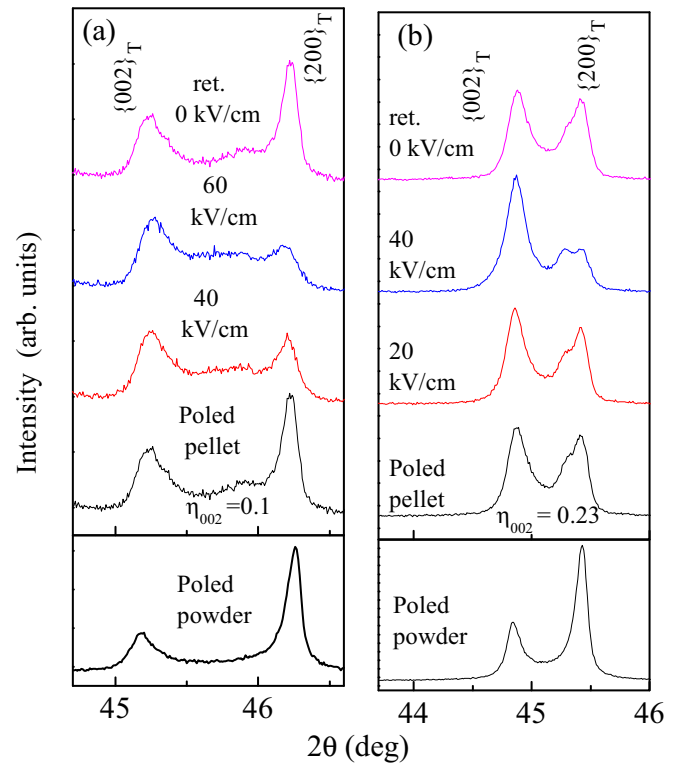


FIG. 8. Evolution of the pseudocubic $\{200\}_{pc}$ XRD Bragg profile with an electric field for the critical compositions of (a) BF-PT:La ($y = 0.30$) and (b) PT-BNH ($x = 0.39$). The XRD pattern *in situ* with an electric field was carried out on poled pellets by applying an electric field in the poling direction. The irreversible domain switching fraction η [calculated from the intensity ratio of 002 and 200 tetragonal peaks; see formula (1)] in the poled pellets of the two specimens is specified.

ingly, the weak cubic peak (indicating the leftover disordered regions left over after poling) shifts to the left as η increases. This implies that domain switching of the majority tetragonal regions elastically pulls/shears the lattice of the in-between disordered regions (manifesting as cubic on the global scale). On decreasing the field, the d spacing of the cubic phase is restored back to its original position together with the reverse switching of the domains. This shows that the critical composition exhibits a strong coupling between the remanent disordered regions and ordered tetragonal regions.

D. Comparison of BF-PT:La and PT-BNH

For better appreciation of the ultrahigh electrostrain in BF-PT:La, a comparative study on the critical composition of PT-BNH was also performed, Fig. 8(b). The critical composition of this series shows unipolar electrostrain of $\sim 0.4\%$ at a field of 60 kV/cm. For the same field BF-PT:La showed almost twice the electrostrain ($\sim 0.80\%$). Two important factors highlight the extraordinary electrostrain in BF-PT:La. (i) After poling PT-BNH shows $\eta \sim 0.24$ which is almost two and a half times that in BF-PT:La ($\eta \sim 0.10$). This implies that the domains are more easily pinned in PT-BNH than in BF-PT:La during their motion in the first application of the unipolar field cycle. (ii) During the subsequent unipolar cycle, we noted,

however, a similar extent of reverse domain switching in both PT-BNH and BF-PT:La. η of PT-BNH increased from 0.24 to 0.47 ($\Delta\eta = 0.23$) when the field was increased from 0 to 40 kV/cm. For BF-PT:La the corresponding increase is 0.1–0.32 ($\Delta\eta = 0.22$) on increasing the field from 0 to 40 kV/cm. The nearly doubled electrostrain in BF-PT:La for a similar level of reverse domain switching can be rationalized by taking into consideration the fact that the tetragonality of BF-PT:La is also nearly double ($c/a-1 = 0.023$) the tetragonality of PT-BNH ($c/a-1 = 0.013$).

E. Discussion

1. Distinction between MPB and non-MPB ferroelectric solid solutions

A recent neutron pair distribution function analysis of a related system $(1-x)\text{PT}-(x)\text{Bi}(\text{Ni}_{1/2}\text{Zr}_{1/2})\text{O}_3$ (PT-BNZ) [19] suggested a gradual change in the local structure from tetragonal to monoclinic with increasing composition (x). Based on the similarity of the local structure of the critical compositions of the PT-BNZ and PT-BS, it was argued that the critical composition of PT-BNZ corresponds to the morphotropic phase boundary. A characteristic feature of the MPB compositions is that, apart from exhibiting coexistence of two ferroelectric structures (say, tetragonal and rhombohedral/monoclinic), they also exhibit considerable positional disorder [19]. The extent of the positional disorder (and hence spatial fluctuation of the polarization on the local scale) can, however, be quantitatively/qualitatively understood only in terms of the departure from a reference structure. For example, if the average symmetry is tetragonal with polarization along [001], the random fields may cause the local polarization to deviate slightly away from [001] in a statistical sense in different unit cells. Similarly, if the average structure is rhombohedral, the positional disorder would manifest as local deviations of the atomic displacements away from the [111] direction. Hence, despite the prevalence of positional disorder, the system is expected to possess a ground-state structure with definite symmetry, upon which the positional disorder is superimposed. This information is crucial for our understanding of the mechanism associated with the large electromechanical response in ferroelectric solid solutions. Since the structure as revealed by XRD is averaged over several unit cells, positional disorder can mask the ground-state symmetry [27]. For example, the cubic phase in PT-BNH and BF-PT:La hides the nature of the ground-state ferroelectric distortion (tetragonal) on the scale of a unit cell. In another ferroelectric solid solution $(1-x)\text{Na}_{1/2}\text{Bi}_{1/2}\text{TiO}_3-(x)\text{BaTiO}_3$, the critical composition ($x = 0.06$) also exhibits a cubic phase. Here, however, the positional disorder is centered around the rhombohedral ($R3c$) distortion [28]. Usher *et al.* have shown a length scale dependent average structure in disordered ferroelectric solid solutions [27]. The enhanced tetragonality in our poled specimens as compared to that of the unpoled specimen [Fig. 4(b)] can be rationalized as another manifestation of length scale dependent average structure. In the unpoled state the correlation length of the tetragonal regions is comparatively less than that when the specimen is poled. This can make the average tetragonal structure exhibit less tetragonality in the unpoled state. In view of the above, the slight change in the pair

distribution function after poling PT-BNH should be treated as readjustment of the bonds on the local length scale as the poling field decreases the extent of positional disorder (Fig. 6). In the case of PT-BS wherein poling does induce a structural change by transforming ~ 15 vol% of the rhombohedral to tetragonal, the PDF fails to show a noticeable change.

That after poling the cubic structure transforms to tetragonal clearly suggests that what appears as a cubic phase on the length scale of XRD is in reality positionally disordered tetragonal regions, and not positionally disordered rhombohedral regions. In the latter scenario, a strong electric field would have increased its correlation length of the rhombohedral regions and make it manifest on the global (XRD) scale. In view of the above, what appears as a “two-phase” (tetragonal + cubic) state in unpoled specimens of PT-BNH is not so in reality. It is rather a manifestation of the coexistence of positionally ordered and disordered tetragonal regions. This scenario is qualitatively different from that in genuine MPB systems (such as the PZT and PT-BS) wherein coexistence of two ferroelectric phases with different symmetries (tetragonal and rhombohedral) does occur. The understanding of this difference has important implications for our understanding of factors that contribute to large electromechanical response in ferroelectric solid solutions. In the absence of interferroelectric instability, the propensity of polarization rotation can no longer be invoked as the dominant mechanism contributing to the large electromechanical response in PT-BNH, BF-PT:La, and the like. Instead of a composition dependent interferroelectric instability, the critical compositions PT-BNH and BF-PT:La are characterized by enhanced positional disorder, without a concomitant change in the ground-state structure. We may note that although the nature of transitions in the relaxor are not well defined [29], they too exhibit temperature induced lattice softening [30] and enhanced elastic susceptibility [31]. However, being thermally driven, the polarization decays very fast in the vicinity of the temperature exhibiting maximum softening and precludes the possibility of realizing large piezoelectric response. It is therefore important that the non-MPB systems like ours should be optimally below the thermal depolarization temperature to have a combination of good polarization and elastic softness [32]. The softening of the Raman mode in the analogous system PT-BNZ [14,19] appears to suggest that the normal to relaxor crossover is associated with some kind of lattice instability, and therefore enhanced elastic compliance. If the effect of lattice softening continues deep in the nonergodic temperature range of the relaxor, then the twin combination of enhanced elastic susceptibility and large polarization can give rise to large piezoelectric response in non-MPB systems. Datta *et al.* have reported that in addition to the large polarization, the critical composition exhibiting the highest piezoelectric response is the one which also exhibits dynamic coupling between the A and B site cations [19].

2. Mechanism of large electrostrain in non-MPB piezoelectric

It is worthwhile to compare the extraordinarily large electrostrain of $\sim 1\%$ in BF-PT:La with the electrostrain $\sim 0.7\%$ reported earlier in a $\text{Na}_{0.5}\text{Bi}_{0.5}\text{TiO}_3$ -based ferroelectric [33]. While both BF-PT:La and the NBT-based system exhibit a

cubic phase in the unpoled state, suggesting a great deal of positional disorder, they behave differently on application of an electric field. The NBT-based ferroelectric exhibits nanometer-sized rhombohedral ($R3c$) and tetragonal ($P4bm$) domain symmetries in the unpoled state. A strong electric field suppresses the nanosized tetragonal domains. Concomitantly, the nanosized rhombohedral domains grow in size [33]. This phenomenon is reversible in the sense that upon removal of the field, the system regains the nanodomain configuration. The large electrostrain in the NBT-based piezoelectric has been associated with the reversible nature of the field driven tetragonal to rhombohedral transformation. This scenario is analogous to the field driven interferroelectric transformation contributing to the enhanced electrostrain at the MPB of PZT [25,34]. This is in marked contrast to what happens in the BF-PT:La composition exhibiting giant electrostrain of $\sim 1\%$. Here the cubic phase transforms irreversibly to tetragonal after experiencing the first field. A small volume fraction of the leftover cubic phase, however, also survives. The large electrostrain in BF-PT:La is therefore primarily due to ferroelastic switching of the tetragonal domains. As our XRD experiment *in situ* with an electric field suggests (Fig. 8), the surviving cubic phase plays a crucial role of providing the restoring force for reverse switching of the tetragonal domains when the field is reduced.

We speculate that the surviving cubic most likely represents the positionally disordered regions in the immediate vicinity of the La site, and it cannot acquire a long-range ferroelectric order even on application of a strong field. When tetragonal domains reorient on application of an applied electric field, the remnant disordered regions are sheared/pulled elastically (as revealed in the XRD pattern via shifting of the cubic peak on the low angle side, [Fig. 8(a)]). These regions tend to restore their original state upon removal of the field. That the relative intensity of the $(002)_T$ and $(200)_T$ tetragonal peaks is also almost restored to value before the field was applied confirms a strong coupling between the long-range ferroelectric domains and the disordered regions for the critical BF-PT:La composition.

3. A-site driven ferroelectrics as non-MPB piezoelectrics

Provided there is a reasonable solid solubility of a non-ferroelectric active cation in a ferroelectric matrix, the ferroelectric system is most likely to degenerate to a relaxor ferroelectric state. For example, beyond a critical threshold, Zr and Sn substitution at the Ti site in BaTiO_3 drives the system towards a relaxor state. The electromechanical response of these compositions is, however, weak as compared to their polymorphic phase boundary counterparts [35]. It appears that not only the correlation length of the polarization, but also the magnitude of the polarization decreases on the local scale as the relaxor state is approached in BaTiO_3 based

systems. This is plausible keeping in view the fact that polarization contribution in BaTiO_3 primarily comes from the Ti-O interaction. In PbTiO_3 and BiMeO_3 ferroelectrics, on the other hand, the A-site cations Pb and Bi are the dominant contributors to the system's polarization. The covalent interaction of the $6s^2$ lone pair electrons of Pb^{+2} and Bi^{+3} with the oxygen polyhedron induces a local polarization which is significantly much stronger than what can be achieved by Ti-O covalent interaction [36]. When such a ferroelectric system is driven towards a relaxor state, the decay in polarization on the local scale may not be as significant as in the case of B-site driven ferroelectric systems (such as BaTiO_3 or KNbO_3). Such systems can continue to show reasonably large polarization in the ferroelectric-relaxor crossover regime, and therefore large electromechanical response by virtue of the enhanced mobility of the ferroelectric domains. The additional contribution may also come from the lattice softening in case the system shows such a tendency around the ergodic-nonergodic temperature. In view of this, non-MPB relaxor ferroelectric systems in the solid solution category $(\text{Pb, Bi})(\text{Me}_I\text{Me}_{II})\text{O}_3$ - PbTiO_3 would be of great interest and worth exploring for large electromechanical response [35].

IV. CONCLUSIONS

In summary we show that large electromechanical response is possible even in non-MPB ferroelectric systems. This possibility can be realized at the ferroelectric-relaxor crossover regime when a strong ferroelectric system (say, Pb/Bi-based ferroelectrics) is driven towards a relaxor state. The compositions in the normal to relaxor crossover regimes turn out to be the critical compositions which can deliver as large electromechanical response as any MPB-based high-performance piezoelectric. Such systems as well have the capability to produce exceptionally large high-field electrostrain if the field-stabilized tetragonal phase exhibits large tetragonality in conjunction with large reverse switching of the ferroelectric-ferroelastic domains. Our study suggests that there lies opportunity to design ferroelectric compositions exhibiting large electromechanical response outside of the conventional MPB framework.

ACKNOWLEDGMENTS

U.S. gratefully acknowledges the Science and Engineering Research Board (SERB), Government of India, for financial support through a SERB-National Post-doctoral Fellowship (Grant No. PDF/2017/000247). R.R. acknowledges SERB of the Ministry of Human Resource Development (Grant No. EMR/2016/001457), and Space Technology Cell of IISc (Grant No. STC-0406) for financial assistance.

- [1] B. Jaffe, W. R. Cook, and H. Jaffe, *Piezoelectric Ceramics* (Academic Press, New York, 1971).
 [2] S.-E. Park and T. R. Shrout, *J. Appl. Phys.* **82**, 1804 (1997).

- [3] M. Ahart, M. Somayazulu, R. E. Cohen, P. Ganesh, P. Dera, H. Mao, R. J. Hemley, Y. Ren, P. Liermann, and Z. Wu, *Nature* **451**, 545 (2008).

- [4] Y. Saito, H. Takao, T. Tani, T. Nonoyama, K. Takatori, T. Homma, T. Nagaya, and M. Nakamura, *Nature* **432**, 84 (2004).
- [5] W. Liu and X. Ren, *Phys. Rev. Lett.* **103**, 257602 (2009).
- [6] T. Takenaka, K. Maruyama, and K. Sakata, *Jpn. J. Appl. Phys.* **30**, 2236 (1991).
- [7] H. Fu and R. E. Cohen, *Nature* **403**, 281 (2000).
- [8] D. Damjanovic, *J. Am. Ceram. Soc.* **88**, 2663 (2005).
- [9] Y. M. Jin, Y. U. Wang, A. G. Khachatryan, J. F. Li, and D. Viehland, *Phys. Rev. Lett.* **91**, 197601 (2003).
- [10] D. Damjanovic, *Rep. Prog. Phys.* **61**, 1267 (1998).
- [11] A. Pramanick, D. Damjanovic, J. E. Daniels, J. C. Nino, and J. L. Jones, *J. Am. Ceram. Soc.* **94**, 293 (2011).
- [12] G. A. Samara, *J. Phys.: Condens. Matter* **15**, R367 (2003).
- [13] Z. Pan, J. Chen, L. Fan, L. Liu, L. Fang, and X. Xing, *J. Appl. Phys.* **112**, 114120 (2012).
- [14] R. Pandey, B. Narayan, D. K. Khatua, S. Tyagi, A. Mostaed, M. Abebe, V. Sathe, I. M. Reaney, and R. Ranjan, *Phys. Rev. B* **97**, 224109 (2018).
- [15] B. Narayan, J. S. Malhotra, R. Pandey, K. Yaddanapudi, P. Nukala, B. Dkhil, A. Senyshyn, and R. Ranjan, *Nat. Mater.* **17**, 427 (2018).
- [16] P. Juhas, T. Davis, C. L. Farrow, and S. J. L. Billinge, *J. Appl. Crystallogr.* **46**, 560 (2013).
- [17] K. V. Lalitha, A. N. Fitch, and R. Ranjan, *Phys. Rev. B* **87**, 064106 (2013).
- [18] R. E. Eitel, C. A. Randall, T. R. Shrout, P. W. Rehrig, W. Hackenberger, and S.-E. Park, *Jpn. J. Appl. Phys.* **40**, 5999 (2001).
- [19] K. Datta, R. B. Neder, J. Chen, J. C. Neuefeind, and B. Mihailova, *Phys. Rev. Lett.* **119**, 207604 (2017).
- [20] S. A. Fedulov, P. B. Ladyzhinskii, I. L. Pyatigorskaya, and Y. N. Venevtsev, *Sov. Phys. - Solid State* **6**, 375 (1964).
- [21] J. Chen, L. Hu, J. Deng, and X. Xing, *Chem. Soc. Rev.* **44**, 3522 (2015).
- [22] S. Bhattacharjee, K. Taji, C. Moriyoshi, Y. Kuroiwa, and D. Pandey, *Phys. Rev. B* **84**, 104116 (2011).
- [23] R. Ranjan and K. A. Raju, *Phys. Rev. B* **82**, 054119 (2010).
- [24] B. Narayan, Y. A. Sorb, B. Loukya, A. Samanta, A. Senyshyn, R. Datta, A. K. Singh, C. Narayana, and R. Ranjan, *Phys. Rev. B* **94**, 104104 (2016).
- [25] R. D. Shannon, *Acta Crystallogr., Sect. A* **32**, 751 (1976).
- [26] M. Hinterstein, J. Rouquette, J. Haines, P. Papet, M. Knapp, J. Glaum, and H. Fuess, *Phys. Rev. Lett.* **107**, 077602 (2011).
- [27] T.-M. Usher, T. Iamsasri, J. S. Forrester, N. Raengthon, N. Triamnak, D. P. Cann, and J. L. Jones, *J. Appl. Phys.* **120**, 184102 (2016).
- [28] R. Garg, B. N. Rao, A. Senyshyn, P. S. R. Krishna, and R. Ranjan, *Phys. Rev. B* **88**, 014103 (2013).
- [29] R. A. Cowley, S. N. Gvasalia, S. G. Lushnikov, B. Roessli, and G. M. Rotaru, *Adv. Phys.* **60**, 229 (2011).
- [30] S. Wakimoto, C. Stock, R. J. Birgeneau, Z. G. Ye, W. Chen, W. J. L. Buyers, P. M. Gehring, and G. Shirane, *Phys. Rev. B* **65**, 172105 (2002).
- [31] S. G. Lushnikov, A. I. Fedoseev, S. N. Gvasalis, and S. Kojima, *Phys. Rev. B* **77**, 104122 (2008).
- [32] M. Acosta, N. Khakpash, T. Someya, N. Novak, W. Jo, H. Nagata, G. A. Rossetti, and J. Roedel, *Phys. Rev. B* **91**, 104108 (2015).
- [33] X. Liu and X. Tan, *Adv. Mater.* **28**, 574 (2016).
- [34] M. Hinterstein, M. Hoelzel, J. Rouquette, J. Haines, J. Glaum, H. Kungl, and M. Hoffman, *Acta Mater.* **94**, 319 (2015).
- [35] A. K. Kalyani, K. Brajesh, A. Senyshyn, and R. Ranjan, *Appl. Phys. Lett.* **104**, 252906 (2014).
- [36] I. Grinberg and A. M. Rappe, *Phys. Rev. Lett.* **98**, 037603 (2007).